PNAS RESEARCH ARTICLE | PHYSICS

Symmetries and synchronization from whole-neural activity in the *Caenorhabditis elegans* connectome: Integration of functional and structural networks

Bryant Avila[a,1], Pedro Augusto[b,c,1], Alireza Hashemi[a,d,e,1], David Phillips[f], Tommaso Gili[g], Manuel Zimmer[b,2], and Hernán A. Makse[a,d,e,h,2]

Affiliations are included on p. 10.

Edited by David Weitz, Harvard University, Cambridge, MA; received September 4, 2024; accepted April 20, 2025

Understanding the dynamical behavior of complex systems from their underlying network architectures is a long-standing question in complexity theory. Therefore, many metrics have been devised to extract network features like motifs, centrality, and modularity measures. It has previously been proposed that network symmetries are of particular importance since they are expected to underlie the synchronization of a system's units, which is ubiquitously observed in nervous system activity patterns. However, perfectly symmetrical structures are difficult to assess in noisy measurements of biological systems, like neuronal connectomes. Here, we devise a principled method to infer network symmetries from combined connectome and neuronal activity data. Using nervous system-wide population activity recordings of the *Caenorhabditis elegans* backward locomotor system, we infer structures in the connectome called fibration symmetries, which can explain which group of neurons synchronize their activity. Our analysis suggests functional building blocks in the animal's motor periphery, providing testable hypotheses on how descending interneuron circuits communicate with the motor periphery to control behavior. Our approach opens a door to exploring the structure–function relations in other complex systems, like the nervous systems of larger animals.

complex networks | fibration symmetries | synchronization | connectome | *Caenorhabditis elegans*

Complex systems depend on an intricate interplay between the dynamical properties of their building blocks and the network structures that link them together. For decades, researchers have endeavored to uncover how the topological attributes of a network could shed light on its dynamical behavior. While several methods have been proposed to elucidate this interplay (1–4), the role of the network's symmetries has garnered considerable attention in recent years (5–12). Identifying and understanding such symmetries has potentially profound implications: Network theory implies that certain symmetrical structures termed fibration symmetries in a graph permit synchronizations (7, 8, 10, 12), a ubiquitously observed phenomenon in brain networks (13). Thus, identifying these symmetries might be crucial for decoding some of the structure–function relationships in a neuronal network.

Fibration symmetry refers to a specific type of symmetry where nodes can be grouped into equivalence classes of balanced colorings based on their input patterns (10, 12, 14). Nodes in the same class receive identical "input trees," which are hierarchical mappings of input connectivity patterns, are proposed to share the same dynamics, and thus can synchronize their behavior. These equivalent nodes are said to belong to the same "fiber" and are also "balanced colorings" of the graph (8). This is formalized through admissible ordinary differential equations (ODEs), which describe the evolution of the system's state (5). Theory ensures that balanced colored nodes with isomorphic input trees following a set of admissible ODEs will evolve in synchrony (7, 8, 12, 15, 16) forming a cluster of synchronization (5, 6). This synchronization can be crucial in various biological systems ranging from gene regulatory networks to brain networks involved in language processing (17, 18). Thus, identifying fibration symmetries provide a prediction in which subsets of nodes potentially exhibit synchronized dynamics.

However, there are technical and conceptual challenges to this theory. Biological networks like connectomes are inherently incomplete, and measuring them is limited by annotation errors, missing links, and noise, yet identifying fiber symmetries is sensitive to small variations in a connectivity matrix. More fundamentally, assuming mathematically perfect symmetries and equivalences of nodes in a biological network is unrealistic. Here,

Significance

Complex biological networks exhibit an intricate relationship between the structural composition of their elements' interaction and the whole system's functionality. This is particularly true in neuroscience, where the multiscale organization of neurons gives place to a multitude of hierarchical functionalities responsible for the nervous system interacting with the environment in which it is embedded. In this study, we focus on the chemical synaptic network of the backward-crawling locomotion circuitry of the worm *Caenorhabditis elegans* to correlate structural clusters of neurons with dynamic patterns of their synchronization. Our findings reveal functional building blocks in the animal's motor periphery, providing testable hypotheses on how descending interneuron circuits communicate with the motor periphery to control behavior.

Author contributions: M.Z. and H.A.M. designed research; B.A., P.A., A.H., D.P., T.G., M.Z., and H.A.M. performed research; B.A., P.A., and A.H. analyzed data; and B.A., P.A., A.H., D.P., T.G., M.Z., and H.A.M. wrote the paper.

The authors declare no competing interest.

This article is a PNAS Direct Submission.

[1]B.A., P.A., and A.H. contributed equally to this work.

[2]To whom correspondence may be addressed. Email: manuel.zimmer@univie.ac.at or hmakse@ccny.cuny.edu.

This article contains supporting information online at https://www.pnas.org/lookup/suppl/doi:10.1073/pnas.2417850122/-/DCSupplemental.

Published June 2, 2025.

we propose that network symmetries represent constraints rather than perfect blueprints for their implementations in individual animals. We aim to address these challenges by studying the interplay of symmetry and synchronization in the locomotor system of the nematode *Caenorhabditis elegans*.

The nematode worm *C. elegans* (19–21)exhibits a small nervous system of just 302 neurons that develop from a stereotypic cell lineage into 118 anatomically and genetically defined cell classes, most of which are composed of a bilaterally symmetrical pair of neurons (e.g., AVAL and AVAR) (22). Its connectome has been fully reconstructed with a synaptic resolution (22–24), and it is tractable for large-scale single-cell resolution neuronal calcium imaging (25, 26). Both, in combination, offer unique opportunities to study structure–function relationships in the nervous system (4). The worm connectome shares many features with connectivity data from larger nervous systems, e.g., rich-club architecture and modularity (24, 27–29). Moreover, neuronal recordings in *C. elegans* revealed nervous system-wide neuronal activity dynamics that exhibit synchronization patterns among well-defined ensembles of neurons(25, 26, 30). These dynamics correspond to motor commands for a set of actions like forward-crawling, backward-crawling, or turning(25, 31). These dynamics are generated in the absence of any known acute time-varying sensory stimuli (25, 26, 30) and can be promoted by arousing conditions, such as environmental oxygen or blue light (32, 33). Moreover, these dynamics can be observed in immobilized animals; even under such conditions, they extend to the motor periphery, incorporating motor neurons, under unconstrained conditions mediating movement execution (30). These features point toward intrinsic mechanisms that drive and maintain synchronous activity states. In accordance, our previous work indicated that rich club architecture and input similarities are crucial architectural features in the connectome that permit synchronized neuronal dynamics(26).

In the present study, we focus on the chemical synaptic network of the backward-crawling locomotion circuitry of *C. elegans* to circumvent some of the technical and conceptual constraints posed by theory and computational limits. In addition, this is a large subpopulation of synchronized neurons which depends almost exclusively on chemical transmission to execute a single behavior. This subnetwork of just 21 individual neurons includes three bilateral pairs of interneurons, AVA, AVE, and AVD, which are situated in the head of the animal and send descending chemical synapses to two classes of motor neurons, termed DA1-9 and VA1-12. These motorneurons form neuromuscular junctions with the dorsal and ventral body wall muscles, respectively, and are required to generate the backward crawling gait (34–36). All chemical synapses in this subnetwork are cholinergic and, with few exceptions, neurons within the same class share similar morphology and gene expression patterns (21, 22, 37). Hence, assuming equivalence among nodes within the same class could be a reasonable simplification.

By leveraging advanced calcium imaging techniques, we first study neuronal dynamics, aiming to identify patterns of synchronization within its backward locomotion circuitry. We then use the observed synchronization dynamics to infer underlying symmetries in the connectome. Given the potential variability in connectomes across individual worms, expecting the universal connectome model to predict the exact neural synchronization across neurons is unrealistic. This variability underscores the necessity of adopting tailored approaches to understand the dynamic behavior from the structure of the connectome. We approach this problem by reconstructing the underlying connectome of *C. elegans* guided by the synchronization dynamics obtained experimentally. This is done by "repairing" the connectivity structure of a typical connectome (27) by solving an appropriately modeled integer linear program to find the minimal number of repairs of the available connectome needed to ensure the observed synchronization dynamics. We aim for a fibration-symmetric connectome that reflects the observed synchronization. This method provides a means to idealize connectomes conceptually. According to interanimal connectome differences reported experimentally in refs. 28 and 38, the threshold for connectome modifications can be taken to not exceed approximately 50%. However, for our final repair solution, we take the stringent threshold of 25% given by animal-to-animal differences found in ref. 27.

To ascertain the robustness and validity of our solutions, we engage in a rigorous testing procedure. We aim to determine the optimality of our solution by reshuffling the neuronal labels in the connectome and revisiting the repair process. We accept our method's solution only if the post-relabeling solutions consistently underperform our primary findings (in over 95% of instances). Our study bridges the gap between structural and functional neuronal data, leveraging the power of symmetries in graph theory to shed light on synchronization dynamics within *C. elegans* and the structure of the connectome underlying this synchronization.

1. Results

In this section, we delineate the pipeline employed throughout our study in a condensed fashion and details are elaborated in *Methods*. Fig. 1 provides an outline of the method to reconstruct the connectome:

1. The process begins with the experimental setup to record neuron activity in Fig. 1*A* with a microfluidic device for immobilization of *C. elegans* enabling nervous system-wide Ca++ imaging with a confocal fluorescence microscope setup.
2. Time series data for activity traces of multiple neurons are recorded simultaneously, as shown in Fig. 1*B*. This procedure is performed on multiple worms under similar conditions.
3. To obtain functional pairwise synchrony matrices, various metrics that capture synchrony are applied to the recorded time series data (Fig. 1*C*).
4. The synchrony matrices shown in Fig. 1*D* are averaged across worms to account for trial-to-trial and/or interindividual variability.
5. A standard thresholding process is then applied to obtain the functional network (Fig. 1*E*) (39, 40). Starting from a disconnected graph, we add links between nodes in decreasing order of weight of the averaged synchrony matrix until every node is in the same connected component. This is done for each averaged matrix.
6. Finally, a consensus matrix is calculated (41) across different methods of synchrony (Fig. 1*F*).
7. A hierarchical clustering algorithm is implemented to find a partition of synchrony clusters (Fig. 1*G*). Each neuron is assigned a color according to its cluster of synchrony. These colors are used as inputs to the repair algorithm in the next step.
8. We formulate and solve a mixed integer linear program (MILP) that finds the minimum number of edges to add or remove from the raw connectome (taken from ref. 27) to produce an ideal fibration-symmetric network that reproduces the coloring in the consensus partition obtained in the previous step (Fig. 1*H*).

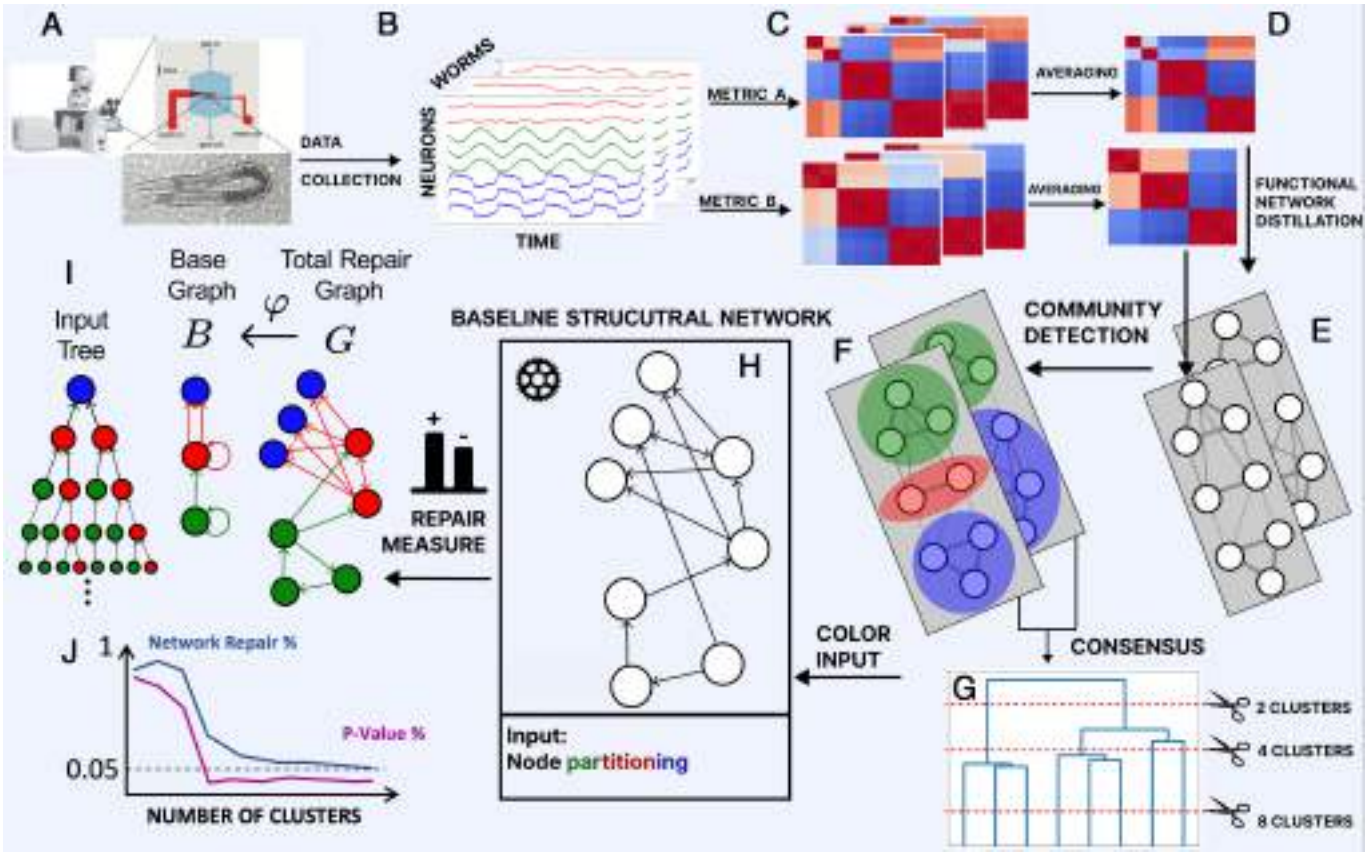

Fig. 1. Pipeline for the structural network repair of the backward locomotion of *C. elegans* based on neural recordings. (*A*) Experimental setup. (*B*) Time series data showing the activity traces of multiple neurons. Traces are color-coded to indicate similar dynamics. (*C*) Matrices of synchronization are obtained from the traces. (*D*) The synchronicity matrices are averaged across worms, accounting for any missing activity traces of individual neurons. (*E*) The percolation procedure was applied to the averaged matrices to obtain the functional network. (*F*) Averaging the functional networks leads to a consensus matrix across different methods of synchrony measured. (*G*) A hierarchical partitioning is implemented to identify clusters of synchronicity. (*H*) MILP repairs the network according to cluster synchronization. (*I*) The solution to the MILP produces an ideal network guided by synchronization. This network can be "collapsed" into its base. (*J*) *P*-value statistics to choose the optimal solution.

9. The network produced by the solution to the MILP is a fibration symmetric connectome with cluster synchronization that reproduces the experimental data. This network can be collapsed into a smaller representation, the base graph, where nodes belonging to the same fiber have isomorphic input trees (Fig. 1*I*). The base graph suggests functional building blocks in the connectome.
10. For each consensus partition, a permutation *P*-value test is performed by permuting node labels and repairing the structural network over 10,000 times. The partition with a significant *P*-value is chosen as the optimal solution (Fig. 1*J*).

1.1. Neuronal Activity Recordings. To simultaneously record calcium activity from interneurons in the head and motor neurons along the entire ventral cord, we modify a recently reported whole nervous system imaging pipeline (30). Briefly, worms expressing the calcium probe NLS-GCaMP6f in a panneuronal fashion, together with NeuroPal multicolor cell identification labels (42), are immobilized in a microfluidic device that positions them in the field of view of a spinning disk confocal microscope. After fast volumetric GCaMP6f imaging, multicolor stacks are taken for cell class identification (see *SI Appendix*, section 1.1 for details).

We generated eight datasets from different young adults well-fed worms. Imaging covered almost the entire body spanning from the head ganglia, the complete ventral cord, and the tail ganglia with single-cell resolution (Fig. 2 *A* and *B*). Animals were recorded for 10 min at approximately three volumes per second. Fig. 2*C* shows a multineuron time series with discernible calcium activity patterns of the neurons selected for this study. These include neurons AVAL/R and AVEL/R, which belong to the major descending interneurons conveying motor commands for backward crawling, as well as the downstream backward crawling motor neurons of the DA and VA classes (see *SI Appendix* section 1.1 for schematic and magnified images). Consistent with previous studies (25, 26, 30), AVA and AVE activity exhibited discrete transitions in their activity patterns, characterized as low, rise, high, and fall states. We previously validated that these states correspond to behavioral states in freely crawling animals; that is, low corresponds to forward crawling, rise and high corresponds to backward crawling, and fall corresponds to turning (25).

Here, we observe that these features are mirrored in the motor periphery (Fig. 2*C*). The mean pairwise correlations among motorneurons and interneurons were high, indicating the strong coupling between them (Fig. 2*D*). During free backward crawling, animals generate a posterior-to-anterior traveling body wave of alternating dorsal–ventral body oscillations. We did not observe any obvious oscillations or activity patterns alternating between the DA and VA motorneurons, which innervate the dorsal and ventral body wall muscles, respectively. Neither did we observe any delay or sequential activation patterns between motor neurons that innervate more posterior to anterior muscles (which

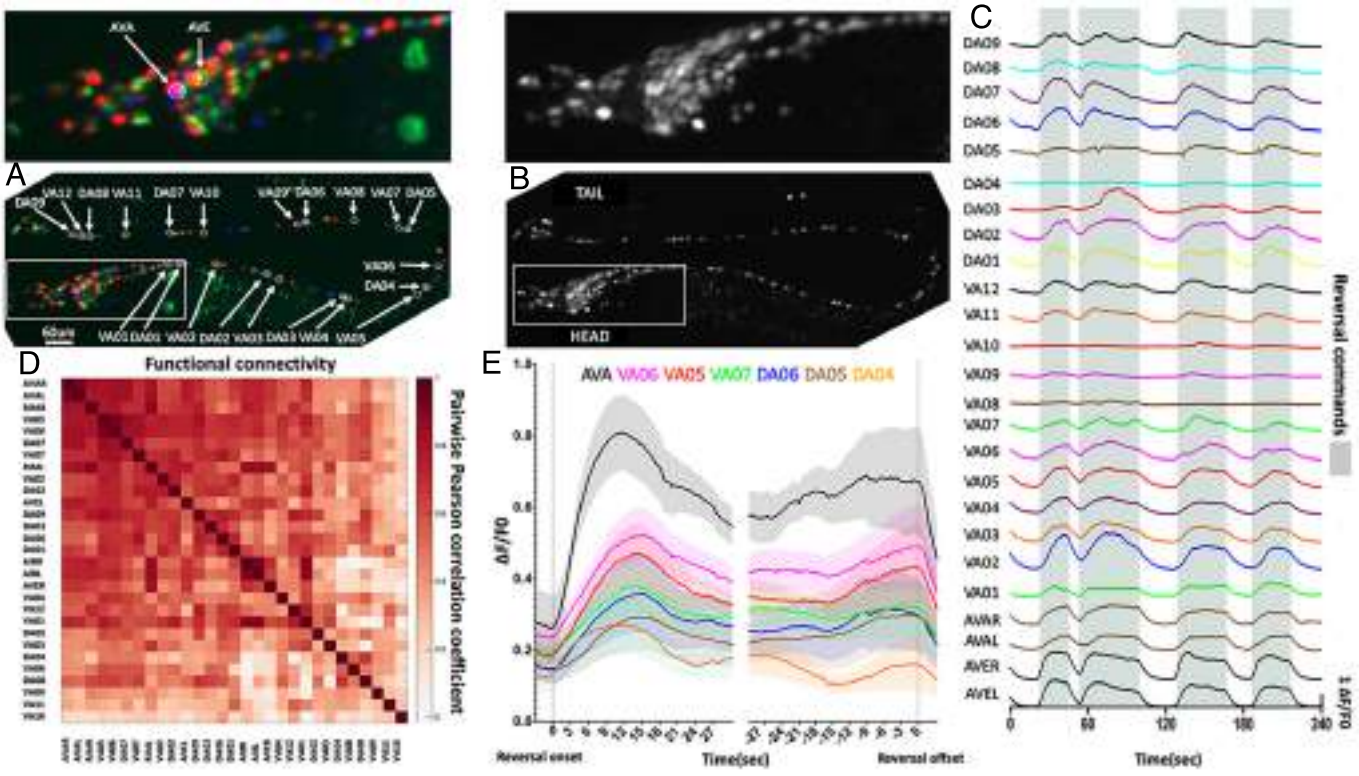

Fig. 2. Whole nervous system recording reveals synchronous motor neuron activity. (*A*) NeuroPAL labeled worm with selected neuronal cell class identities indicated. (*B*) The same worm as in (*A*) showing NLS-GCaMP6f labeling. (*C*) Activity time series (DF/F0) of selected, gray shading indicates reversal command states defined by AVAL activity. (*D*) Pairwise Level of Synchronization (*LoS*) among selected neurons. Each matrix entry is the average of $N = 3$ to 8 pairwise observations. (*E*) The triggered average (±SEM) to reversal command onset (*Left*) and offset (*Right*) are both defined by reference neuron AVAL. Three example neurons of each VA and DA motor neuron class are shown. Averages calculated across recordings represent the dynamics that we observe in our datasets; neurons are relatively aligned in time, but there are substantial differences regarding their amplitudes.

is indicated by the index number in their name, $n = 1$ most anterior, $n = 12$ most posterior). However, all motor neurons follow the rise and fall states of the AVA descending command interneuron (Fig. 2*E*). In conclusion, under our experimental immobilization conditions, A-class motorneurons do not generate gait-related patterns in their Ca++ activity profiles. However, they appear to respond to descending motor commands from their presynaptic interneurons reliably. This feature and the absence of movement, hence the lack of proprioceptive inputs, makes the present setup particularly suitable for studying neuronal dynamics dependent on internal neuronal circuit interactions (*Discussion*).

1.2. Cluster Synchronization Measures from the Functional Network. Assessing the synchronization of two or more signals recorded simultaneously involves various methods tailored to the specific characteristics and similarities of interest. This results in a diverse array of techniques aiming to capture synchronization through different approaches (43). These techniques are generally classified into four primary groups based on their focus: time domain versus frequency domain and methods that account for directional dependencies versus those that do not (*SI Appendix*, section 1.2 and Table S1).

Correlation is a robust measurement for coherence in neuronal data obtained via calcium imaging (25, 44, 45) (*SI Appendix*, section 1.2). In addition to correlation, to quantify the amount of synchronicity between two signals, we implement the Level of Synchronicity (*LoS*) measure introduced in refs. 46 and 47 (*SI Appendix*, section 1.3).

Matrices of synchronization and correlation are computed for each of the $N = 8$ worms under study, capturing the synchronous activities observed within each individual as depicted in Fig. 1*C*. To obtain a representative overview of synchronicity across the entire set of worms, these individual matrices are averaged per type, i.e. for each value of σ (Fig. 1*D*). However, compiling these averaged matrices require care, particularly in instances where the activity of individual neurons are missing for specific worms. Therefore, we calculate the average by averaging over worms for a particular metric type and divide each element (neuron-pair functional measurement) in the summed matrix by the number of times they appear together across the whole cohort of worms.

Each element in the averaged matrix contains information on a neuron pair synchronous relationships used to construct functional networks composed of all the neurons for the backward locomotion gait. We follow standard thresholding procedures (18, 39, 40) to build the functional network. Through this method, we purge the functional data to only contain the strongest links leading to a functional network, as seen in Fig. 1*E*. Using this network, we identify neuron cliques that are synchronized via community and cluster detection algorithms.

A group of neurons that are more synchronous to each other than other neurons belonging to different groups is considered equivalent to a CS of neurons. We apply cluster and community detection algorithms to extract these functionally synchronous clusters of neurons from the functional network using two methods:

- Clique synchronization (18): It decides whether a node belongs to a synchronous clique if the average value of the edges of the functional network inside the clique is bigger than any of its outside edges (*SI Appendix*, section 1.4).
- Louvain community detection (48): It decides the number of clusters and the number of nodes in each cluster by optimizing the modularity function as given by *SI Appendix*, Eq. **4**, which is solely cluster dependent.

The result of applying these methods to a LoS correlation matrix is seen in Fig. 3 *A* and *B*, which results in a functional network with the node partition as seen in Fig. 3*C*. The nodes with the same colors belong to the same cluster synchronization, as can be seen since they share thicker edges than edges between nodes of different colors.

The clusters obtained using the LoS measure at different parametric values produce various motor-neuron partitionings. We only keep those that are unique among the 39 results for the range of σ between 0.01 and 0.20. This is done for each of the two cluster/community detection methods. The number of unique partitionings for each method can be seen in the table within Fig. 3*E*.

1.3. Consensus Synchronous Clusters. We construct 44 metrics to obtain synchronization information: 39 LoS matrices and five types of correlation measures (Pearson, Spearman, and Kendall coefficient, distance correlation, and covariance). We combine these metrics with the two functional clustering methods mentioned in *SI Appendix*, section 1.4 (clique synchronization and Louvain) to create 88 possible partitionings. Then, a consensus is created following the methods developed in ref. 41 to leverage the information obtained from all the partitionings. To achieve this, each partitioning, which consists of n clusters of synchronous neurons, is used to create a co-occurrence matrix, which is simply a matrix with n diagonal blocks, one for each synchronous group, with value 1, and with all other values outside these blocks set to zero (Fig. 3*D*). These matrices are summed up and normalized. The resulting consensus matrix is depicted in Fig. 3*G*. Through this, the sets of neurons that appear in the same synchronous group more frequently than with other neurons appear with higher values. This consensus avoids putting each partitioning in competition with the other and instead compiles them into a globally agreed-upon result (41).

The consensus matrix, called X (Fig. 3*G*), has optimal leaf ordering of its rows and columns. Such is produced by the hierarchical clustering Ward metric (also known as Ward's minimum variance method), applied to the dissimilarity matrix $1 - X$ (as seen in Fig. 3*F*). This metric aims to minimize the total within-cluster variance. The goal is to choose the successive clustering steps to minimize the increase in the total within-cluster variance.

From this consensus, we can obtain various partitionings depending on where the dendrogram is sliced. When the dendrogram is sliced at a value of 3 we obtain three major groups as observed in the thick block structure in Fig. 3*G*. Each block can be further divided into smaller diagonal blocks if we reduce the threshold. For instance, 7 clusters are observed for a cutoff at 1.05 represented by the smaller blocks in Fig. 3*G*. In the next sections, we will see that this partitioning is the optimal solution obtained by the reconstruction algorithm with the least amount of modifications to convert the baseline Varshney connectome into a fibration symmetric solution. Some neurons cannot connect physically as reported in the literature (22, 24, 27). For instance, DA neurons can only send chemical connections to the dorsal side the dorsal side but can receive them from both the ventral and dorsal side. We use these restrictions in our algorithm.

All these partitions are the input to the mixed integer linear programming algorithm that we designed to reconstruct the connectome with a minimal number of modifications with the constraint of not adding physically impossible connections, as explained next.

1.4. Balanced Coloring Partitions and Functional Network Clustering. To develop the optimization algorithm to reconstruct the connectome to satisfy the synchronization found in the previous section, we need to introduce the concept of "balanced coloring" and the fibration of the graph. Fig. 4*A* shows an example of a graph with a balanced coloring.

Let $\mathcal{C} = C_1, \cdots, C_K$ be a partition of the nodes of a network $G = (V, E)$ with V vertices and E edges. We identify each cluster C_k with a different color and K is the total number of colors. A "balanced coloring" is a coloring of the graph such that each node with color k in cluster C_k is connected (by edges of the same type) to the same number of nodes with color j in cluster C_j, for $1 \leq k, j \leq K$. That is, nodes of the same color receive the same colors from their neighbors (Fig. 4*A*, center)

Translated into the terminology of dynamical systems, a system of differential equations for the state variables of each node $V_i(t)$ can be interpreted as a "message passing" process of passing colored messages through the edges of the graph. Since two nodes i and j with the same color received the same colors (messages) from their neighbors, we can think, intuitively, that they will synchronize their activity $V_i(t) = V_i(t)$, forming a synchronous cluster. This intuition is made mathematically rigorous (15) through the theory of fibrations (10, 12).

Traditionally, a way to formalize the balanced coloring partitions is through the automorphisms of the graph forming its symmetry group (5, 6). In this case, the orbits of the automorphisms of the graph are the balanced colors. However, not all balanced colorings are orbits. Many biological networks contain no automorphisms, yet, they display a nontrivial balanced coloring partition with many colors (12, 16). This is exemplified in Fig. 4*A*. The graph has no automorphisms (except for the trivial identity) but has a balanced coloring that reduces the graph to a base with just two nodes. This balanced coloring is only captured by the fibration.

The graph fibration formalism introduced in ref. 10 is a more general formalism that captures all balanced coloring partitions of the graph. Graph fibrations are a particular case of fibrations between categories introduced previously by Grothendieck (49) and are formal generalizations of graph automorphisms.

A graph fibration (shown on the *Right* of Fig. 4*A*) is a morphism of the graph that collapses every cluster of synchronized balanced colors (called "fibers") into a single representative node in the base graph B while conserving the "lifting property" defined in *SI Appendix*, section 1.5. This transformation leaves invariant the dynamics in the graph and captures the maximal symmetries of the network. It is then called a symmetry fibration (12). Here, we propose that fibers represent potential functional modules or building blocks in a network of neurons.

1.5. Fibration Symmetry Driven Repair Algorithm. The clusters of synchronous neurons found in Section 1.3 are used to repair the raw chemical synapses connectome of the backward locomotion gait of *C. elegans* provided by Varshney et al. (27) (plotted in Fig. 5*B*). We develop an optimization mixed linear integer program to modify this network by adding or

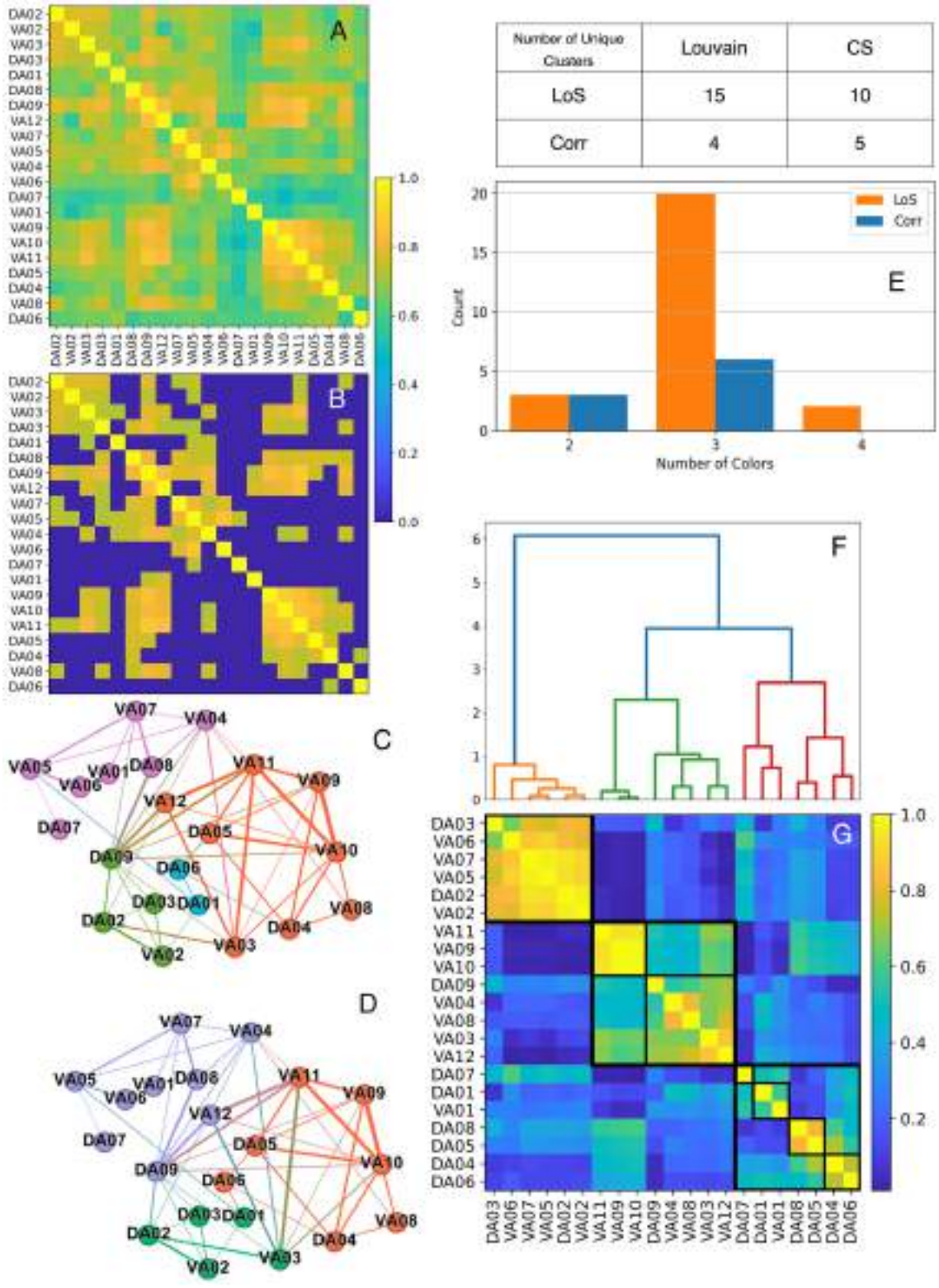

Fig. 3. Results of the clustering analysis. (*A*) Average of $N = 8$ *LoS* matrices at $\sigma = 0.16$. (*B*) Functional matrix thresholding adds matrix elements in decreasing order of values until the matrix corresponds to a graph where all of the nodes are in one connected component. (*C*) The functional matrix is then converted into an indirect graph. Node colors show clustering using the Clique Synchronization method. Edge thickness relates to values in the *LoS* matrix. (*D*) Same as the graph in panel (*C*) but with the Louvain method partitioning nodes. (*E*) Distribution of synchrony cluster numbers among unique partitionings. Given the neurons' high monotonic and synchronous relationships, *LoS* measurement helps distinguish partitionings with more clusters via Ca2+ signal amplitude. Partitionings are applied to 39 *LoS* matrices and five correlation matrices using Distance, Pearson, Kendall, Spearman, and Covariance. *LoS* row matrices are obtained from unique σ values ranging from 0.01 to 0.20 in 0.005 steps. (*F*) Dendrogram of averaged co-occurrence matrices using Ward-metric hierarchical clustering. Three major groups of backward motor neurons are observed in green, blue, and red. (*G*) Averaged co-occurrence matrices show two levels of hierarchical clustering. Diagonal blocks with thick lines are the high level 3 cluster view from the dendrogram, while those with thin lines are subclusters corresponding to colored neuron groups within the three major clusters. These 7 clusters correspond to a dendrogram slice at 1.05.